Available online at www.sciencedirect.com
ScienceDirect
International Journal of Heat and Mass Transfer 51 (2008) 707–716
International Journal of HEAT and MASS TRANSFER
www.elsevier.com/locate/ijhmt

Transition from annular flow to plug/slug flow in condensation of steam in microchannels

Xiaojun Quan, Ping Cheng *, Huiying Wu

School of Mechanical and Power Engineering, Shanghai Jiaotong University, 800 Dong Chuan Road, Shanghai 200240, PR China

Received 23 February 2007; received in revised form 24 April 2007
Available online 3 July 2007

Abstract

A visualization study has been conducted to investigate the transition from annular flow to plug/slug flow in the condensation of steam in two different sets of parallel microchannels, having hydraulic diameters of 90 μm and 136 μm, respectively. The steam in the parallel microchannels was cooled on the bottom by forced convection of water and by natural convection of air from the top. It is found that the location, where the transition from annular flow to plug/slug flow takes place, depends on mass flux and cooling rate of steam. The effects of mass flux and cooling rate on the occurrence frequency of the injection flow in a single microchannel, having a hydraulic diameter of 120 μm and 128 μm, respectively, are investigated. It is found that two different shapes of injection flow occur in the smooth annular flow in microchannels: injection flow with unsteady vapor ligament occurring at low mass flux (or high cooling rate) and injection flow with steady vapor ligament occurring at high mass flux (or low cooling rate). It is also found that increase of steam mass flux, decrease of cooling rate, or decrease of the microchannel diameter tends to enhance instability of the condensate film on the wall, resulting in occurrence of the injection flow further toward the outlet with an increase in occurrence frequency.

Keywords: Silicon microchannel; Condensation; Injection flow; Slug frequency

1. Introduction

During the past decade, much work has been carried out to study the transition from annular flow to plug/slug flow in two-phase flow with and without phase-change in macrochannels. For example, Dukler [1,2] studied the formation process and models of slug flow after the occurrence of gas–liquid interface fluctuations. It was found when the height of liquid layer at the bottom of tube rose to the top of tube, it formed a liquid bridge tamping the flow of gas in the tube and thus producing slug flow. As a result, an asymmetric flow pattern was formed during the transition process. On the other hand, transition from annular flow to slug/bubbly flow in condensation of refrigerants in a macrotube was studied by Soliman [3], who showed that gravity plays an important role in the transition process.

Recently, a great deal of attention has been given to the study of phase-change heat transfer in minichannels and microchannels because of its application to two-phase compact heat exchangers and microheat exchangers [4]. Garimella and co-workers [5–8] have carried out measurements and visualization studies on condensation of refrigerants in minichannels ($1\text{ mm} < D_h < 4\text{ mm}$). They categorized four major flow regimes as annular, intermittent, wavy and dispersed, which were further subdivided into 16 flow patterns. Revellin et al. [9] reported that with the decrease of the hydraulic diameter, the elongated bubble gradually took a symmetrical shape in condensation of R-134a in a 0.5 mm channel. This indicated that the flow characteristics were independent of channel orientation with respect to gravity, which is due to the fact that surface tension is predominant in microchannels. Serizawa et al. [10] performed steam–water two-phase flow experiments in a microchannel

* Corresponding author. Tel./fax: +86 21 6293 3107.
E-mail address: pingcheng@sjtu.edu.cn (P. Cheng).

0017-9310/$ - see front matter © 2007 Elsevier Ltd. All rights reserved.
doi:10.1016/j.ijheatmasstransfer.2007.04.022

Nomenclature

A	cross-section area	x	vapor quality
A_{sf}	glass top surface area	W_b	bottom width
Co	condensation number	W_t	top width
f	frequency	W_t/H	aspect ratio
G	mass flux		
h	heat transfer coefficient	*Subscripts*	
H	gap between bottom and top	in	inlet
h_{fg}	latent heat	o	outlet
L	total length of channel	c	cooling water
Q	heat transfer rate	w	wall
t	time	v	steam
T	temperature	sf	glass top surface
Z	transition location	amb	ambient air
μ	viscosity		

with a 50 μm I.D. silica capillary tube. They observed that stratified flow did not appear in the microchannel, while bubbly flow, slug flow, liquid ring flow and liquid droplet flow existed in the microchannel. Tabatabai et al. [11] presented a flow transition map for two-phase flow with phase-change heat transfer in micro-tubes, and suggested that flow pattern changes according to a new criteria when surface tension dominates. Teng et al. [12] showed that interface instability of condensate film is induced by surface tension and shear force, and the latter is due to difference in vapor and liquid film velocity. It was found that the effect of surface tension on film instability depends on the wavenumber. The surface tension stabilizes interface if dimensionless wavenumber is greater than 1; otherwise, it has a destabilizing effect. On the other hand, the shear force always has a destabilizing effect on film instability. Most recently, Wu and Cheng [13] studied flow patterns of steam condensation in silicon microchannels, and discovered that injection flow occurred during the transition from annular flow to slug/bubbly flow. They pointed out that the appearance of the injection flow is a unique characteristic of the condensation flow in microchannels.

In this paper, we have carried out further experimental studies to investigate injection flow during condensation in microchannels. A flow pattern map, in terms of heat transfer rate versus mass flux, is drawn for transition from annular flow to slug–bubbly flow in condensation of steam in parallel microchannels with hydraulic diameters of 136 μm. The effects of mass flux and cooling rate of steam on the location at which injection flow occurred and its occurrence frequency are investigated.

2. Experimental setup and methods

2.1. Experiment setup

As shown in Fig. 1, the experimental setup consisted of three major components: a steam generation system, a test section and a visualization system. Steam produced by an electric boiler at a prescribed pressure first flowed through a thermally insulated buffer tank (in order to reduce pressure fluctuations in the case of unsteady boiler operation). Then, it flowed through the connecting tubes, outside of which was wrapped by a band heater to prevent vapor condensing inside the tubes. It entered filters and the microchannels in the test section, which was cooled by a cooling water circulation system with a thermostatic water cabinet to ensure the inlet water at selected temperatures. Finally, the condensate from the test section was discharged into a container, which was placed on an electronic balance. The amount of condensation heat transfer in the test section was regulated by the inlet temperature and the flow rate of subcooled water. If the stream was not completely condensed at the exit of the test section, a postcondenser downstream of the test section was used. An energy balance on the postcondenser provided a redundant and independent validation of vapor quality at the exit of the test section, which could be used to verify heat transfer calculation.

Fig. 2 shows the test section used for the investigation of the transition from annular to plug/slug flow in condensation of steam in the microchannel. The test section was fabricated from a silicon wafer with a single or parallel microchannels of trapezoidal cross-sections with different sizes as shown in Table 1. N1 and N2 are two sets of parallel microchannels, having a hydraulic diameter of 90 μm and 136 μm, respectively, which were etched in the silicon wafer to reduce errors of heat transfer calculation. N3, N4, and N5 are three sets of a single microchannel etched in the silicon wafer so that no flow interaction from neighboring channels affects the condensing flow. Each of the microchannels was 60 mm long with a trapezoidal cross-section. The top side of the silicon wafer was bonded with a borosilicate glass cover using anodic bonding technology to allow the visualization study and to ensure microchannels were air-tight. The bottom side of the silicon wafer was installed with five evenly distributed microthermocou-

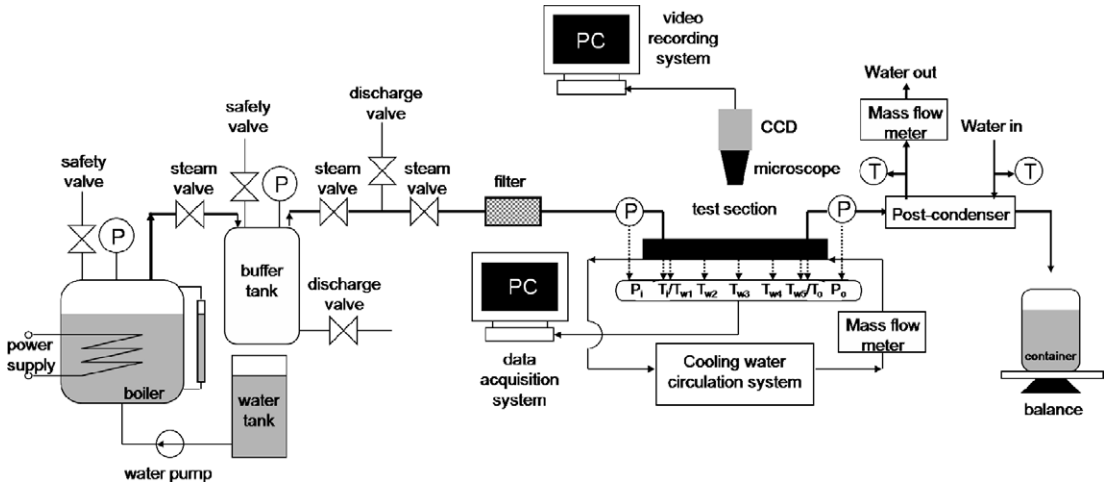

Fig. 1. Experimental system.

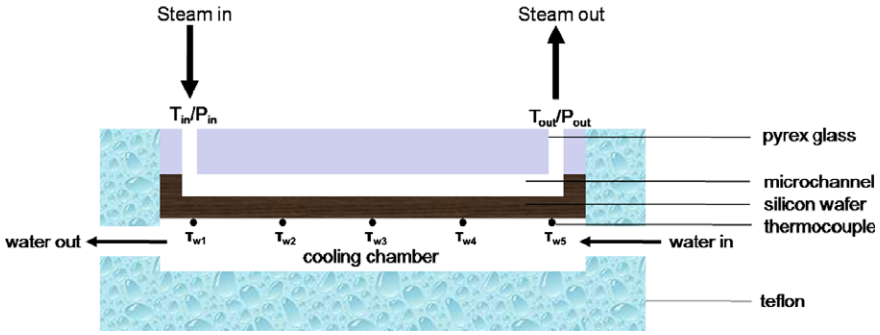

Fig. 2. Test section.

Table 1
Geometric parameters of microchannels

Channel specifications	D_h (μm)	W_t (μm)	W_b (μm)	H (μm)	Aspect ratio (W_t/H)	Number of channels	Channel shape
N1	90	500	427.8	51	9.80	8	Trapezoidal
N2	136	300	144.2	110	2.72	8	Trapezoidal
N3	120	427	320.8	75	5.69	1	Trapezoidal
N4	128	600	493.8	75	8.00	1	Trapezoidal
N5	128	268	112.2	110	2.44	1	Trapezoidal

ples (T-type) for measuring wall temperatures of the microchannels.

To facilitate steam condensation in the microchannels, the bottom side of the silicon wafer was in direct contact with the cooling water. The temperature and the pressure of the steam and cooling water at the outlets and inlets were measured with microthermocouples and pressure transducers, respectively. Accurate measurements of mass fluxes hold the key to the successful execution of microchannel experiments because of small mass rates. To get rid of non-condensable gases in the steam and to ensure that mass flux measurements are steady, it is important to eliminate non-condensable gases in the steam completely. Mass flux was calculated from the mass and time interval of two sequential droplets collected by a container on an electronic balance under steady conditions. All of the temperature, pressure, and flow rate signals were acquired by an Agilent34970A data acquisition system, which were transferred to the computer for data reduction.

To observe condensation flow in the silicon microchannels, microscopic lenses (Nikon 50i) and high-speed CCD (X-stream™ Xs-4) were installed above the microchannels of the test section. A recording rate of 5000 fps was chosen during visualization, which was sufficient to record the transition from annular flow to slug/bubbly flow process. The pictures recorded by a high-speed CCD camera together with data for temperature, pressure and flow rate were analyzed.

2.2. Data reduction

The condensation number, Co, is defined as

$$Co = \frac{Q}{m_v h_{fg}} = \frac{Q}{GAh_{fg}}, \quad (1)$$

where Q is the amount of condensation heat transfer rate in the tube, m_v is the mass rate of steam, and h_{fg} is the latent heat of vapor. Thus, Co is a measure of effectiveness of condensation process: the higher is Co, the larger is the cooling rate. If steam is completely condensed at the exit, Q can be calculated from

$$Q = m_v(h_{vi} - h_{vo}), \quad (2a)$$

where h_{vi} and h_{vo} are the inlet enthalpy of the steam and the outlet enthalpy of the condensate, respectively.

If the stream is not completely condensed at the exit, then the following expression can be used to calculate Q

$$Q = m_c c_p(T_{co} - T_{cin}) + Q_{env}, \quad (2b)$$

where Q_{env} is heat transfer rate dispersing to the environment and m_c is the mass flow rate of cooling water, which was obtained with the aid of an electronic balance; c_p is the specific heat of cooling water; $(T_{co} - T_{cin})$ is the temperature difference of the inlet and outlet of cooling water. If two-phase flow exists in the outlet, Eq. (1) becomes

$$Co \simeq 1 - x, \quad (3)$$

where x is the vapor quality which has a value less than or equal to one.

2.3. Heat loss calibration

Heat loss experiments were performed after the test loop had been built. In order to measure heat loss from the test section, a series of fully condensed tests was performed and Q_{env} was calculated from

$$Q_{env} = Q_s - Q_c = m_v(h_{vi} - h_{vo}) - m_c c_p(T_{co} - T_{ci}). \quad (4a)$$

A heat loss calibration chart was constructed by plotting heat loss Q_{env} versus the temperature difference between the pyrex glass top surface T_s and ambient air T_{amb} as

$$Q_{env} = (hA_{sf})\Delta T_{amb}, \quad (4b)$$

where $\Delta T_{amb} = T_{sf} - T_{amb}$, A_{sf} is the glass top surface area, and h is the natural convection heat transfer coefficient from the glass top surface to the ambient air. A chart for Q_{env} versus ΔT_{amb} was plotted. During the experimental runs, this chart was used to calculate the actual heat carried away by the microchannel array. It was found that less than 7% of the heat transferred from the steam to the wall was lost to the environment. Based on an error analysis [14], the uncertainty in the condensation heat transfer rate Q in parallel microchannels and the condensation number Co can be calculated to be 5.6% and 6.8%, respectively.

3. Experiment results and discussion

3.1. Visualization result

Fig. 3 is a sketch of condensation flow pattern transition in the microchannels and Fig. 4 are photos of flow patterns for corresponding positions. Similar graphs have been presented by Wu and Cheng [13] from these photos, it can be seen that after the saturated steam had entered in the silicon microchannels with their wall cooled by cooling water, the flow pattern changed from mist flow, annular flow, injection flow, plug/slug flow and to bubbly flow along the microchannel sequentially.

Fig. 4a shows that mist flow with vapor and water coexisting with each other at the inlet. The white bright drops are water droplets condensed on the top surface of microchannels because of the lower ambient temperature. With the increasing amount of coagulated droplets on the cooler walls, mist flow gradually changed to annular flow. At the downstream of the annular flow, liquid bridges began to form in the condensing liquid film on the cooler walls. Meanwhile, the vapor core shrank and the speed of vapor phase was increased. When the surface tension and viscous force between steam and liquid was sufficient to overcome inertial force of vapor, injection flow occurred as shown in Fig. 4c, which is a transition separating the annular flow (a shear-dominated flow) and the plug/slug flow (a surface tension-dominated flow). After the breakup of injection flow (as shown in Fig. 4d), Taylor bubbles began to appear, forming plug/slug flow downstream as shown in Fig. 4e. It should be noted from Fig. 4e that the receding angle on the right of the vapor bubble is less than the advancing angle on the left of the bubble, which is in agreement with the contact angle hysteresis [15]. Subsequently, the plug/slug flow became isolated spherical bubbles (Fig. 4f) because

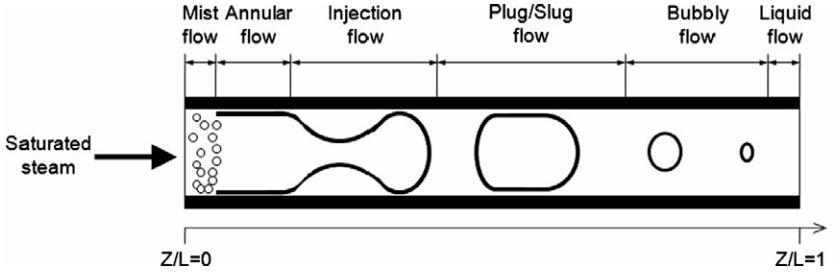

Fig. 3. Sketch of condensation flow patterns in microchannels.

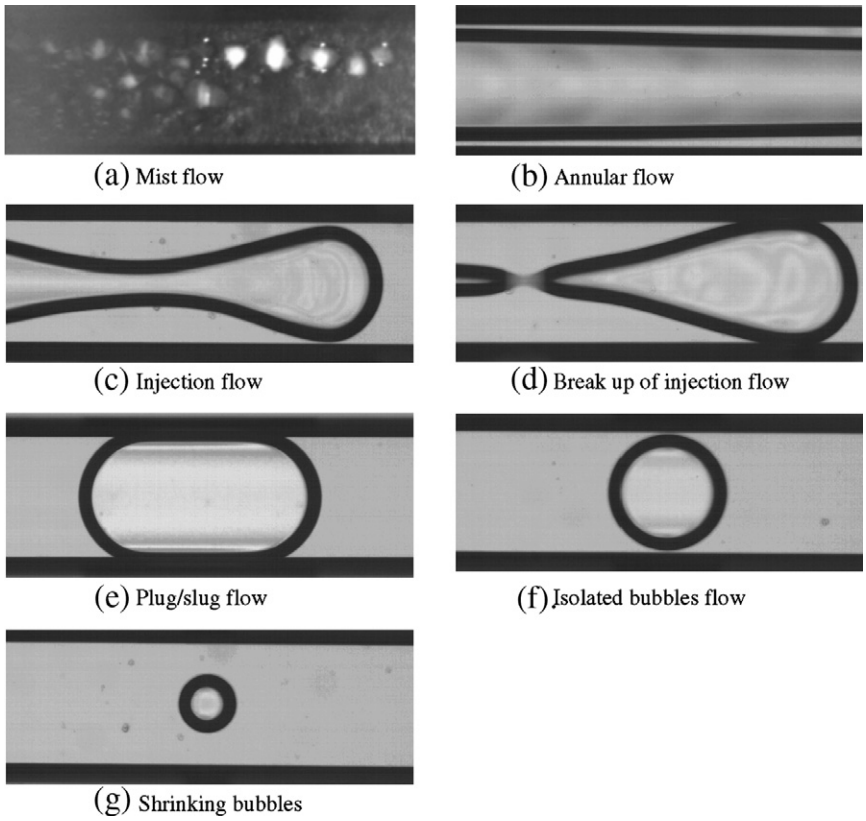

Fig. 4. Visualization photo of flow pattern in different sections of silicon microchannels.

of the continuous cooling from the walls of the microchannel. Finally, isolated bubbles were gradually condensed and shrank and submerged in the condensate further downstream as shown in Fig. 4g.

The occurrence of the injection flow in a smooth annular flow in a microchannel is strongly self-locked at a certain frequency. Fig. 5 shows that two modes of bubble breakup in the smooth annular flow in the microchannel having a hydraulic diameter of 120 μm with a trapezoidal cross-sectional area. This process generates a continuous streaming of microbubbles with perfectly homogeneous and controllable size downstream. Fig. 5a is the first mode with unsteady vapor ligament, corresponding to the case of low mass flux of steam (or high cooling rate), whereas Fig. 5b is the second mode of injection flow with steady vapor ligament, corresponding to the case of high mass flux of steam (or low cooling rate). In general, the second type has a higher frequency of bubble breakup than the first type. Both modes of breakup consist of two distinct stages for bubble generation: the expansion stage and the detachment stage, which is similar to those described by Sevilla et al. [16] for bubble formation in a coflowing of air–water stream. The first mode consists of the unsteady ligament expansion stage (characterized by the radial growth of an vapor ligament left attached to annular vapor liquid interface after the pinch-off of a bubble), and the ligament collapse stage (characterized by the formation of a neck which propagated downstream, became thinner and finally breakup). In comparison with the first mode, the second mode has a steady vapor ligament like a needle, whose length and circular radius will vary corresponding to different flow and heat transfer conditions. When the vapor velocity was increased or cooling rate was decreased, the ligament became longer, while its radius became smaller. At the same time, the occurrence frequency increased as well.

3.2. Transition from annular to plug/slug flow

As mentioned before, the injection flow in microchannels can be considered as the transitional flow from annular flow to slug/bubbly flow. In this experiment, it was found that the location of breakup point Z of the injection flow depends on the mass flux of the steam G and the condensation heat transfer rate Q (or in dimensionless form Co). The occurrence of the injection flow was observed using a high-speed CCD. It is estimated that the errors of mass flux and the location of Z were 4.8% and 6.8%, respectively.

3.2.1. Effects of mass flux of steam

Fig. 6 shows the variation of the dimensionless distance Z/L (with L being the length of the microchannel) with the condensation number Co at three different mass fluxes of steam: $G = 165\ \mathrm{kg/m^2\,s}$, $194\ \mathrm{kg/m^2\,s}$ and $243\ \mathrm{kg/m^2\,s}$, respectively. Note that $Z/L = 0$ means that the microchannel is fully occupied by plug/slug flow and single-phase

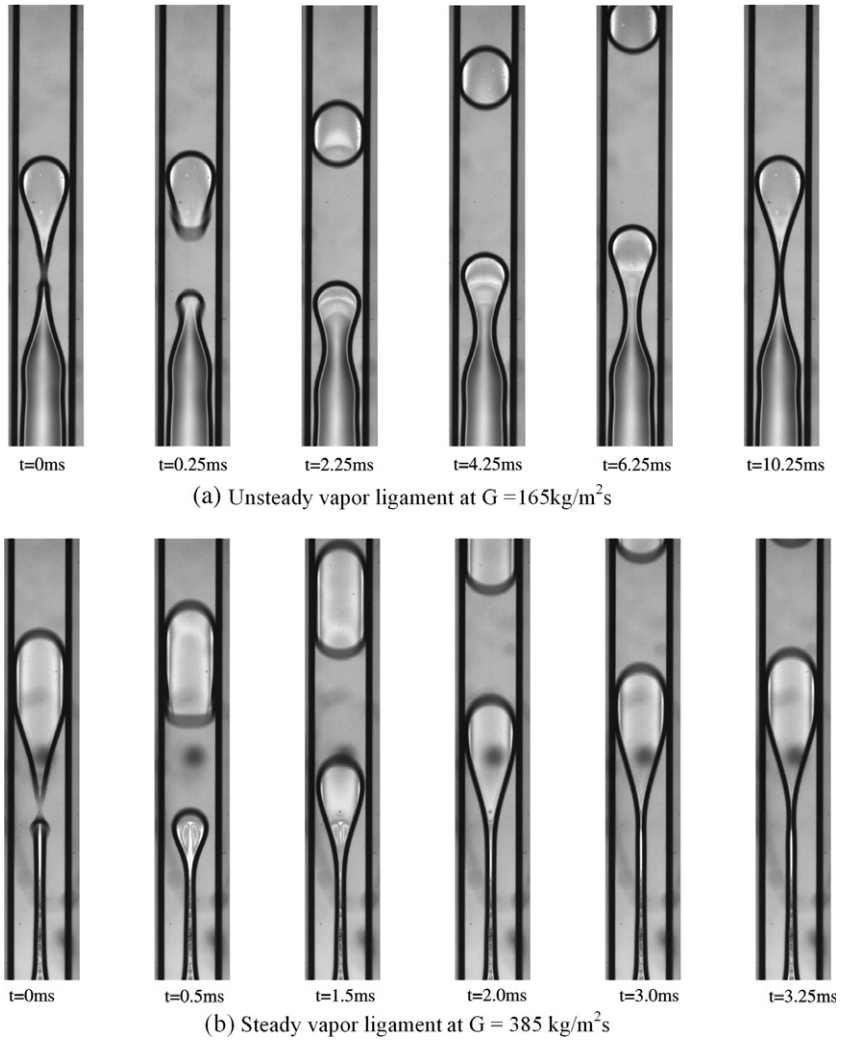

Fig. 5. Two modes of injection flow in a microchannel (N3) with $D_h = 120$ μm: (a) for low mass flux of steam (or high cooling rate) and (b) for high mass flux of steam (or low cooling rate).

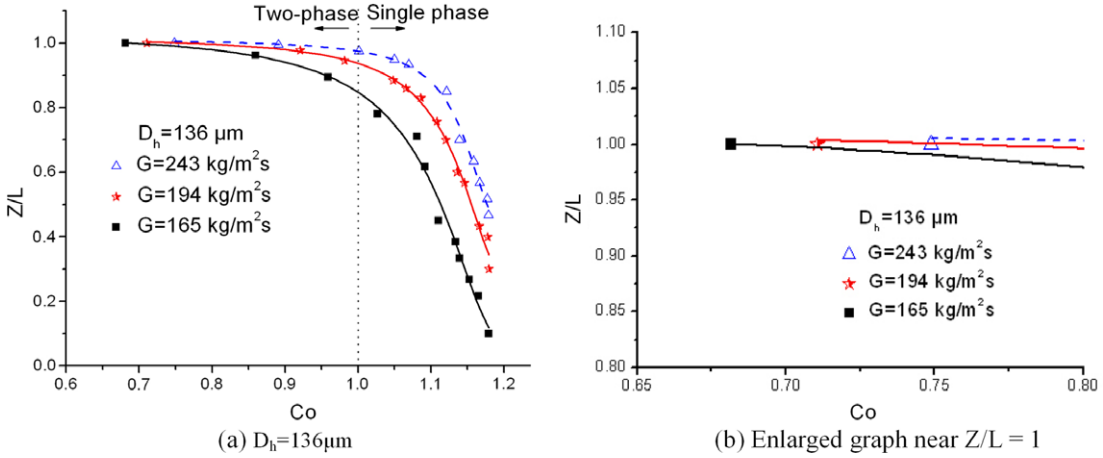

Fig. 6. Effects of mass flux of steam on Z/L at different Co in microchannels (N2) of diameter 136 μm.

liquid, while $Z/L = 1$ means that the microchannel is fully occupied by the annular flow. It can be seen from Fig. 6 that (i) at a constant Co, Z/L increases with the increase in G, meaning that the location of breakup point of injection flow will move toward the outlet, i.e. the annular flow regime in microchannels will be expanded and the slug/

bubbly flow regime will be shrank as the value of G is increased. But if the mass flux of steam is decreased, the whole situation will reverse; (ii) at a constant G, Z/L increases with the decrease in the condensation number, meaning that injection flow occurs further downstream, and the annular flow regime is expanded, and (iii) at $Z/L = 1$, Co increases with the increase of G (see Fig. 6b). According to Eq. (3), this means that the quality (x) at the transition point in the same microchannel is smaller at the higher value of G; (iv) $Co \approx 1$ is criterion whether two-phase flow or liquid phase exists at the outlet. $Co < 1$ means that two-phase flow exists at outlet, i.e. the microchannel is occupied by the annular flow and slug/bubbly flow sequentially. On the other hand, $Co > 1$ means that steam is completely condensed at outlet. i.e. all flow patterns (including mist flow, annular flow, injection flow, plug/slug flow, and isolated bubbles) are present in the microchannel, and (v) Z/L approaches zero at a sufficiently large but finite value of Co.

3.2.2. Effects of microchannel diameter

Fig. 7a shows that the effect of the microchannel diameter on the location of the injection flow at $G = 165$ kg/m^2 s and Fig. 7b is the enlarged graph for Z/L near 1. It can be seen from Fig. 7b that at the same value of G, with the decrease in hydraulic diameter of microchannel Co number slightly decreases at $Z/L = 1.0$. According to Eq. (3),this means that at transition from annular to plug/slug flow in microchannels, the quality (x) increases with the decrease of hydraulic diameter at same mass flux. This is consistent with the previous findings by Garimella et al. [17].

A flow pattern map in terms of Q versus G for condensation flow in a microchannel with a hydraulic diameter of 136 μm is presented in Fig. 8, where the annular flow regime exists below the curve, while the plug/slug flow regime exists above the curve. The seven data points were taken at $Z/L = 1$ including the three data points for $G = 165$ kg/m^2 s, 194 kg/m^2 s, 243 kg/m^2 s which were taken from Fig. 6b. According to Eq. (1), the ratio of heat flow rate to mass flux is proportional to Co. It follows that the increase in the slope of the curve as G is increased in Fig. 8 indicating that Co increases with the increase of G.

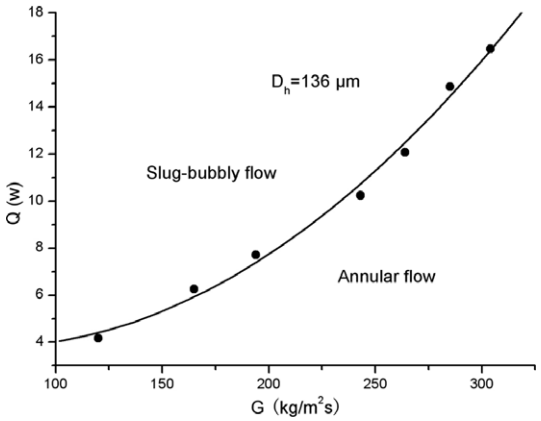

Fig. 8. Flow patterns of annular flow and plug/slug flow in a microchannel (N2) having a diameter of 136 μm.

3.3. Frequency of injection flow in smooth annular flow

In order to minimize flow interaction effects from neighboring microchannels at the headers, experiments were conducted in two sets of single microchannel numbered as N3 and N4 (having a length of 60 mm) in Table 1. It is estimated that the error of the frequency measurements was less than 5%.

3.3.1. Effects of mass flux of steam and cooling rate

Fig. 9 shows the effects of mass flux and cooling rate of steam on the occurrence frequency of the injection flow in the N4 microchannel ($D_h = 128$ μm), where smooth annular flow (see Fig. 4b) existed before injection flow occurred. It is shown that the occurrence frequency of the injection flow increases as the steam mass flux is increased. This is because higher mass flux induced instability, leading to higher occurrence frequency of the injection flow. It is also shown from Fig. 9 that higher cooling rate leads to lower

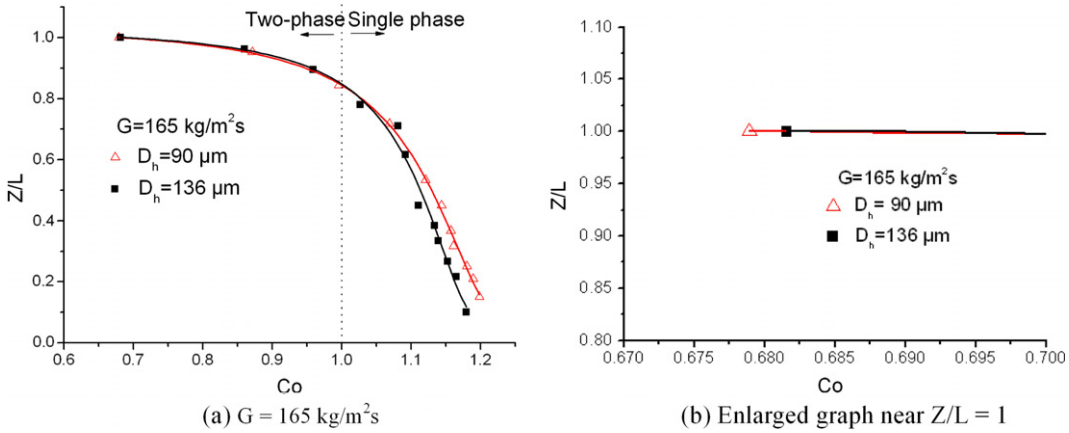

Fig. 7. Effects of microchannel diameter on Z/L at different cooling rates at $G = 165$ kg/m^2 s.

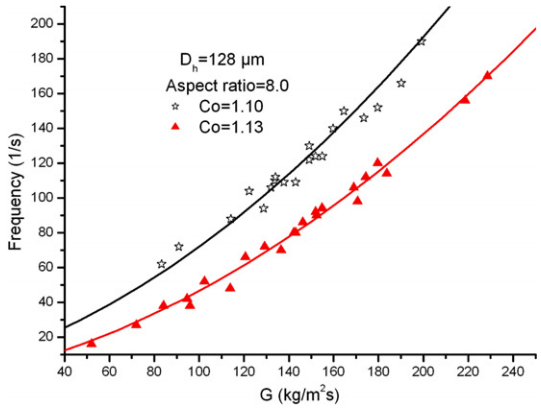

Fig. 9. Effects of steam mass fluxes on occurrence frequency of injection flow at different *Co* numbers in a microchannel (N4).

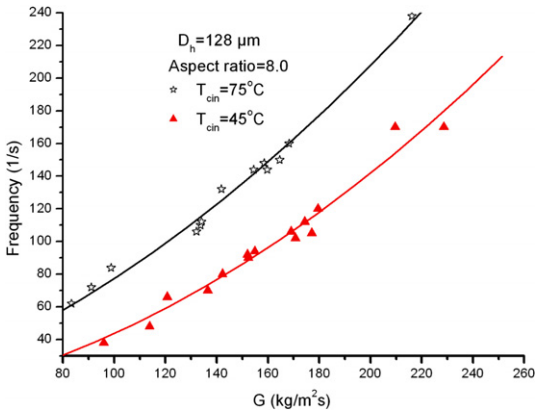

Fig. 11. Effects of inlet cooling water temperatures on occurrence frequency of injection flow at different mass fluxes of steam in a microchannel (N4).

occurrence frequency. This is because interfacial condensation tends to reduce the interface instability [18].

Fig. 10 shows the effect of cooling rate on the occurrence frequency of the injection flow at two different mass fluxes. For a sufficient large cooling rate, complete condensation will occur at the inlet, meaning that vapor is condensed immediately into liquid without injection flow. So the occurrence frequency of injection flow will approach zero asymptotically, when the cooling rate is sufficiently large as shown in Fig. 10. Again, it is shown from this graph that higher occurrence frequency of injection flow at higher steam mass flux, which is consistent with the trend in Fig. 9.

Fig. 11 shows the effect of the inlet temperature of the cooling water on the occurrence frequency of the injection flow in the N4 microchannel. It is shown that the occurrence frequency of the injection flow at inlet temperature of 45 °C is lower than those for inlet temperature of 75 °C (at the same cooling water flow rate of 120 g/min). This is because the inlet of temperature of 45 °C has a higher cooling rate than those with an inlet temperature of 75 °C. Consequently, the occurrence frequency of injection flow with an inlet temperature of 45 °C is lower than those with an inlet temperature of 75 °C according to the conclusion from Fig. 10. It is shown that the occurrence frequency of the injection flow increased with the mass flux, which is consistent with the conclusion from Fig. 9.

3.3.2. Effects of microchannel diameter

Fig. 12 shows the effect of microchannel hydraulic diameter on the occurrence frequency of injection flow. As expected, the smaller the diameter, the higher is the occurrence frequency of the injection flow at the same mass flux. This is because the surface tension effect is more important in a smaller diameter microchannels. Also, according to Fig. 7, the quality (x) at the transition point from annular flow to plug/slug flow in microchannels increases with the decrease of hydraulic diameter at the same mass flux. This increase in vapor quality leads to faster vapor velocity in the microchannel with smaller hydraulic diameter at the same mass flux. The increase of vapor velocity also enhanced interface instability, leading to higher occurrence frequency of the injection flow.

3.4. Injection flow in wavy annular flow

Lee et al. [19] speculated that the cross-sectional shape of the microchannel would affect the instability of two-

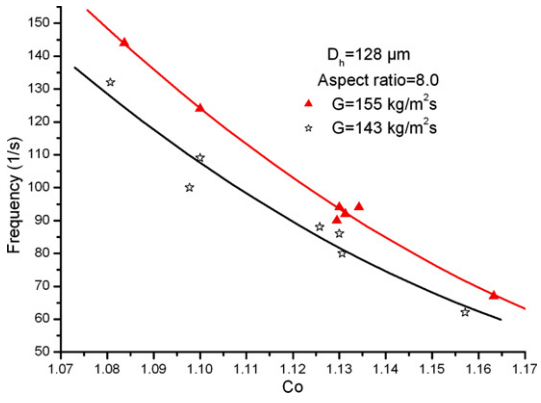

Fig. 10. Effects of *Co* number on occurrence frequency of injection flow at different mass fluxes of steam in a microchannel (N4).

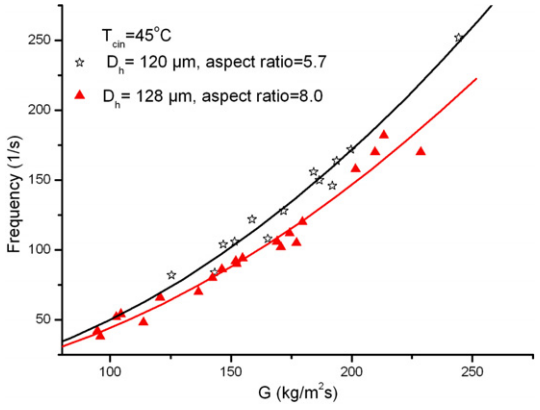

Fig. 12. Effects of microchannel hydraulic diameter on occurrence frequency of injection flow at different mass fluxes.

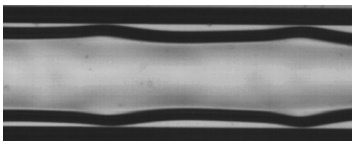

Fig. 13. Photo of wavy annular flow in N5 microchannel.

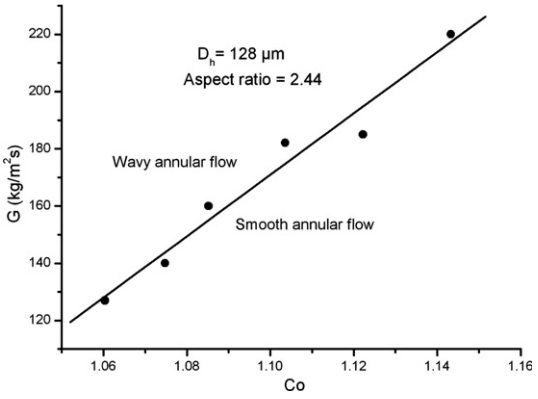

Fig. 14. A flow pattern map for smooth and wavy annular flows in a single microchannel (N5) having a diameter of 128 μm.

phase flow in microchannels. In the present condensation experiment, it was observed that the cross-sectional shape of the microchannel did affect the condensation flow pattern. Although both N4 and N5 had the same hydraulic diameter of 128 μm, the cross-sectional shapes of these two microchannels were different. N4 microchannel had a trapezoidal shape with a shallow depth, while N5 had a cross-section closer to a square shape. Although the wavy annular flow as shown in Fig. 13 occurred under certain conditions of heat flux and mass flux in the N5 microchannel, wavy annular flow never occurred in the N4 microchannel. This illuminates that the cross-sectional shape of the microchannel has a significant effect on flow instability. Fig. 14 is a flow map showing the smooth annular and wavy annular flow regimes in the N5 microchannel. Since the position at which injection flow occurred was unsteady in the wavy annular flow in the N5 microchannel and the time interval and the size of bubbles generated varied with time, the occurrence frequency of the injection flow could not be measured.

4. Concluding remarks

With the aid of a microscope and a CCD camera, condensation flow patterns and the occurrence of injection flow in silicon microchannels with several different hydraulic diameters at different mass fluxes of steam and cooling rate of water have been observed and analyzed. The effects of the mass flux of steam and the microchannel hydraulic diameter on the dimensionless location of injection flow breaking point versus dimensionless condensation number are investigated. A flow pattern map in terms of heat transfer rate versus mass flux for the annular flow regime and the slug–bubbly flow regime in microchannels having $D_h = 136$ μm is presented. The effects of inlet cooling water temperature, *Co* number and microchannel diameter on occurrence frequency of injection flow at different mass fluxes of steam are investigated. It is found that hotter inlet water temperature, higher mass flux of steam or smaller diameter microchannel enhances condensate film instability, leading to higher occurrence frequency of the injection flow and moves the injection flow further toward the outlet. At the same vapor mass flux, higher occurrence frequency occurs in a microchannel with smaller hydraulic diameter because of the effect of surface tension and different quality value at transition point from annular flow to slug/bubbly flow. It is also found that the cross-sectional shape of the microchannel has significant effects on the instability of condensation flow in the microchannel.

Acknowledgements

This work was supported by the National Natural Science Foundation of China through Grant Nos. 50536010 and 50476017, as well as by Shanghai Municipal Science and Technology Committee through Grant No. 05JC14025.

References

[1] Y. Taitel, A.E. Dukler, A model for predicting flow regime transitions in horizontal and near horizontal gas–liquid flow, AICHE J. 22 (1976) 47–55.
[2] E. Abraham, A.E. Dukler, G. Martin Hubbard, A model for gas–liquid slug flow in horizontal and near horizontal tubes, Ind. Eng. Chem. Fundam. 14 (1975) 337–346.
[3] H.M. Soliman, Analytical and experimental studies of flow patterns during condensation inside horizontal tubes, Ph.D. Dissertation, Kansas State University, 1974.
[4] P. Cheng, H.Y. Wu, Mesoscale and microscale phase-change heat transfer, Adv. Heat Transfer 39 (2006) 469–573.
[5] J.W. Coleman, S. Garimella, Two-phase flow regimes in round, square and rectangular tubes during condensation of refrigerant R134a, Int. J. Refrig. 26 (2003) 117–128.
[6] J.W. Coleman, S. Garimella, Visualization of two-phase refrigerant flow during phase change, in: 34th National Heat Transfer Conference, Nhtc2000-12115, 2000.
[7] J.W. Coleman, S. Garimella, Two-phase flow regime transitions in microchannel tubes: the effect of hydraulic diameter, in: Proceedings of ASME Heat Transfer Division HTD-V, vol. 366, 2000, pp. 71–83.
[8] S. Garimella, Condensation flow mechanisms in microchannels: basis for pressure drop and heat transfer models, Heat Transfer Eng. 25 (2004) 104–166.
[9] R. Revellin, V. Dupont, T. Ursenbacher, J.R. Thome, I. Zun, Characterization of diabatic two-phase flows in microchannels: flow parameter results for R-134a in a 0.5 mm channel, Int. J. Multiphas. Flow 32 (2006) 755–774.
[10] A. Serizawa, Z. Feng, Z. Kawara, Two-phase flow in microchannels, Exp. Therm. Fluid Sci. 26 (2002) 703–714.
[11] A. Tabatabai, A. Faghri, A new two-phase flow map and transition boundary accounting for surface tension effects in horizontal minature and microtubes, Trans. ASME 123 (2001) 958–968.
[12] H. Teng, P. Cheng, T.S. Zhao, Instability of condensation film and capillary blocking in small-diameter-thermosyphon condensers, Int. J. Heat Mass Transfer 42 (1999) 3071–3083.
[13] H.Y. Wu, P. Cheng, Condensation flow patterns in silicon micro channels, Int. J. Heat Mass Transfer 48 (2005) 2186–2197.

[14] S.J. Kline, The purposes of uncertainty analysis, J. Fluid. Eng. 107 (1985) 153–160.
[15] V.P. Carey, Liquid–Vapor Phase-change Phenomena, Hemisphere, Washington, 1992.
[16] A. Sevilla, J.M. Gordillo, C. Martinez-Bazan, Bubble formation in a coflowing air–water stream, J. Fluid Mech. 530 (2005) 181–195.
[17] S. Garimella, J.D. Killion, J.W. Coleman, An experimentally validated model for two-phase pressure drop in the intermittent flow regime for circular microchannels, J. Fluid. Eng. 124 (2002) 205–213.
[18] S.H. Chan, Y.S. Wang, C.C. Tan, The effect of mass transfer on Kelvin–Helmholtz instability at the gas–liquid interface of a sonic reacting and non-reacting gas jet submerged in a liquid, Int. J. Heat Mass Transfer 37 (1994) 1123–1132.
[19] M. Lee, Y.Y. Wong, M. Wong, Y. Zohar, Size and shape effects on two-phase flow patterns in microchannel forced convection boiling, J. Micromech. Microeng. 13 (2003) 155–164.